Distributed Synchronization of Heterogeneous Oscillators on Networks With Arbitrary Topology

Enrique Mallada, *Member, IEEE*, Randy A. Freeman, and Ao Kevin Tang, *Senior Member, IEEE*

***Abstract*—Many network applications rely on the synchronization of coupled oscillators. For example, such synchronization can provide networked devices with a common temporal reference necessary for coordinating actions or decoding transmitted messages. In this paper, we study the problem of using distributed control to achieve phase and frequency synchronization of a network of coupled heterogeneous nonlinear oscillators. Not only do our controllers guarantee zero-phase error in steady state under arbitrary frequency heterogeneity, but they also require little knowledge of the oscillator nonlinearities and network topology. Furthermore, we provide a global convergence analysis, in the absence of noise and propagation delay, for the resulting nonlinear system whose phase vector evolves on the n-torus.**

***Index Terms*—Coupled oscillators, distributed control, nonlinear control, synchronization.**

I. Introduction

ACHIEVING temporal coordination among different networked devices is a fundamental requirement for the successful operation of many engineering systems. For example, it is necessary in communication systems to recover transmitted messages [1] in sensor networks for coordinating wakeup cycles [2] or achieving temporal measurement coherence [3], and in computer networks to preserve the causality of distributed events [4]. Almost ubiquitously, such coordination is accomplished by providing each node of the network with its own local oscillator (LO) and then compensating its phase and frequency (using information received from other devices on the network) to achieve a common temporal reference.

Legacy applications, such as public-switched telephone networks and cellular networks, use a centralized hierarchical synchronization scheme with high-precision oscillators that have relative frequency errors ranging from 0.01 to 4.6 parts per million (ppm) [5], [6]. For several reasons, however, these traditional synchronization architectures have become increasingly unsuitable for newer distributed applications. For example, traditional methods can break down with the failure of only a few nodes. In addition, many newer applications use inexpensive oscillators having errors as high as 100 ppm [7]. Thus, a synchronization protocol designed for these newer applications should satisfy two essential requirements: 1) it should be distributed and independent of the network topology (each node should use only its neighbors' oscillator information to adjust it own oscillator) and 2) it should be robust to wide variations and uncertainty in the specifications of the oscillators used throughout the network.

A variety of synchronization algorithms has been proposed along these lines, jointly inspired by collective synchronization in physics and biology [8]–[11] and cooperative control in engineering networks [12], [13]. One possible solution is to use monotonically increasing time sources (e.g., clocks) and update their times based on offset information [14]–[22] to achieve a common *absolute* time reference (clock synchronization). This is suitable for applications in computer networks where a reference to an absolute time is needed (e.g., distributed databases). Another solution is to use periodic time sources (e.g., oscillators) interconnected with phase comparators [23]–[25] or pulse-coupling [26]–[28], where the objective is to achieve a common *relative* time reference (phase synchronization) that enables temporal coordination within the network (e.g., waking up simultaneously).[1]

While the theoretical study of clock synchronization is fairly mature, with solutions that can provide zero offset error synchronization on networks with arbitrary heterogeneous frequencies [4] and asynchronous updates [22], little is known about the phase synchronization counterpart. For example, most phase synchronization solutions present nonzero steady-state phase differences in the presence of frequency heterogeneity [23]–[28] with convergence guarantees limited to idealized scenarios, such as homogeneous frequencies [29]. The only exception is [25] which can guarantee phase synchronization for complete graph topologies. Thus, whether or not such systems can synchronize for arbitrary networks and arbitrary frequency heterogeneity has remained an open question [24].

In this paper, we provide a positive answer to this question under very general conditions. We propose two distributed controllers that can achieve phase synchronization for a network of arbitrarily interconnected oscillators, under mild assumptions on the oscillator and phase comparator characteristics. For example, we allow the instantaneous frequency of each oscillator to be a highly uncertain nonlinear function of the local control input, a model consistent with most analog oscillators [such as voltage-controlled oscillators (VCOs) or complementary

Manuscript received September 17, 2014; revised November 25, 2014; accepted February 27, 2015. Date of publication May 1, 2015; date of current version March 16, 2016. This work was supported by ONR under Grant N00014-12-1-1055. Recommended by Associate Editor N. Elia.

E. Mallada is with California Institute of Technologuy, Pasadena, CA 91125 USA (e-mail: mallada@caltech.edu).

R. A. Freeman is with the Electrical Engineering and Computer Science Department, Northwestern University, Evanston, IL 60208-3118 USA (e-mail: freeman@eecs.northwestern.edu).

A. K. Tang is with the School of Electrical and Computer Engineering, Cornell University, Ithaca, NY 14853 USA (e-mail: atang@ece.cornell.edu).

Color versions of one or more of the figures in this paper are available online at http://ieeexplore.ieee.org.

Digital Object Identifier 10.1109/TCNS.2015.2428371

[1] Although one can use clock synchronization to achieve phase synchronization by simply mapping the linear times onto the circle using a modulo operator, this approach can lead to undesirable transients if the phases keep wrapping around the circle as the linear times synchronize. For this reason, we consider these to be separate synchronization problems, each suitable for different application areas.

metal–oxide semiconductors (CMOS) oscillators]. Also, unlike existing work, we allow the set of oscillator frequencies to be bounded, so that each oscillator may operate within a prescribed frequency range, even during the transient part of the response. Finally, we allow flexibility in the choice of the phase comparator responses, rather than assuming as in [25] that they are sinusoidal. We only require that the measured phase difference is noiseless and can be obtained without propagation delay.

The main contribution of this paper is a novel nonlinear convergence analysis that leverages recent results on the stability of equilibria of homogeneous-frequency coupled oscillators [29]. In particular, our controllers are based on a Hamiltonian dynamic system defined on the graph in which each local minimum of the energy function represents a synchronized trajectory. Each controller employs a different mechanism to dissipate energy and thereby converge to a synchronized solution. Furthermore, we show that any trajectory that is synchronized in frequency but not in phase must be unstable and that the phase-synchronized trajectory is almost-globally stable.

II. Notation and Terminology

We let $\mathbb{T} = \mathbb{R}/2\pi\mathbb{Z}$ denote the unit circle, regarded as the Lie group of angle addition. We equip $\mathbb{T}$ with the usual Riemannian metric which defines the distance $d(p,q)$ between two points $p, q \in \mathbb{T}$ to be the length of the shorter of the two arcs connecting them. Given a set $S \subseteq \mathbb{T}$, we define the diameter of S to be $\operatorname{diam}(S) = \sup_{p,q\in S} d(p,q)$ (so that $\operatorname{diam}(\mathbb{T}) = \pi$). For $p \in \mathbb{N}$, we let $\mathbb{T}^p$ denote the Cartesian product of p circles. For $i \in \{1,\dots,p\}$, we let ∂_i denote the unit vector field pointing in the counterclockwise direction on the ith factor of $\mathbb{T}^p$ (which we write simply as ∂ when $p = 1$). Because these unit vector fields form an ordered basis for the tangent space of $\mathbb{T}^p$ at each point, we can represent tangent vectors for $\mathbb{T}^p$ as elements of $\mathbb{R}^p$, that is, as coordinate vectors with respect to this basis. Moreover, all Jacobian matrices of mappings defined on $\mathbb{T}^p$ will be representations of the differential with respect to this basis.

All graphs in this paper will be simple, undirected, connected graphs having n vertices (with $2 \leqslant n < \infty$) and m edges (with $m \geqslant n-1$). We represent such a graph $\mathbb{G}$ as a pair $\mathbb{G} = (\mathcal{V}, \mathcal{E})$ for a vertex set $\mathcal{V}$ and edge set $\mathcal{E}$. We label and order the vertices and edges, writing $\mathcal{V} = \{1,\dots,n\}$ and $\mathcal{E} = \{1,\dots,m\}$, where each edge $k \in \mathcal{E}$ is an unordered pair of distinct vertices $k = \{i,j\} \subset \mathcal{V}$. For each vertex $i \in \mathcal{V}$, we let $\mathcal{N}_i$ denote the following indexed set of neighbors of i:

$$\mathcal{N}_i = \{(j,k) \in \mathcal{V} \times \mathcal{E} : k = \{i,j\}\}. \tag{1}$$

Thus, $(j,k) \in \mathcal{N}_i$ if and only if $(i,k) \in \mathcal{N}_j$, that is, if and only if edge k connects vertices i and j.

III. Problem Statement and Results

We consider a network of controlled oscillators in which each oscillator shares the current value of its phase with its immediate neighbors. The purpose of the controller design is to guarantee frequency and phase synchronization of the interconnected system. We adopt the classical phase-locked loop (PLL) structure for each controlled oscillator [23], [30]. This structure consists of three components connected in feedback, as illustrated in Fig. 1: a base oscillator, a phase comparator, and a loop filter. The base oscillator is a physical device (such as a VCO) whose frequency is determined dynamically by means of a control signal; the phase of each controlled oscillator system is simply the phase of its base oscillator. The phase comparator produces a phase error signal by comparing its own phase with the phases of its neighbors. Finally, the loop filter produces the control signal from the phase error.

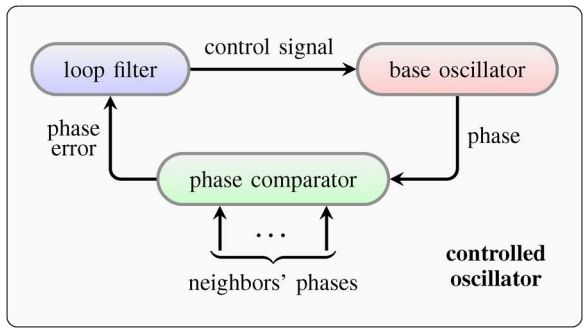

Fig. 1. PLL components of a controlled oscillator.

We represent the network of oscillators by a graph $\mathbb{G} = (\mathcal{V}, \mathcal{E})$ in which each vertex is a controlled oscillator and each edge indicates an exchange of phases between neighboring vertices.

We represent the phase of oscillator i at time $t \in \mathbb{R}$ by $\varphi_i(t) \in \mathbb{T}$, and we write the phase vector signal for the entire network as the column vector

$$\varphi = [\varphi_1 \ \dots \ \varphi_n]^T \in \mathbb{T}^n. \tag{2}$$

We define a synchronization measure $\delta\varphi$ to be the diameter of the finite subset of $\mathbb{T}$ consisting of the n phases φ_i

$$\delta\varphi = \operatorname{diam}\{\varphi_1,\dots,\varphi_n\} \in [0,\pi]. \tag{3}$$

Note that if $\delta\varphi < 2\pi/3$, then the n phases φ_i all lie within an arc of length $\delta\varphi$. Therefore, a small value of $\delta\varphi$ represents a tight clustering of the oscillator phases, and these phases are all identical when $\delta\varphi = 0$. This diameter (3) is a worst-case measure of synchronization, rather than an average measure, as a single outlier can make this diameter large. The following definition describes our design goal.

Definition 1: Let $\mathcal{I} \subset \mathbb{R}$ be an interval. The network of oscillators achieves *almost-global synchronization within* $\mathcal{I}$ when for almost all initial states (including the initial oscillator phases and any initial loop filter states), the trajectories of the system satisfy:

- **asymptotic frequency synchronization**: there exists a constant $\omega^\star \in \mathcal{I}$ such that $\dot{\varphi}_i(t) \to \omega^\star$ as $t \to \infty$ for each $i \in \mathcal{V}$;
- **asymptotic phase synchronization**: $\delta\varphi(t) \to 0$ as $t \to \infty$;
- **constrained frequencies**: $\dot{\varphi}_i(t) \in \mathcal{I}$ for all $t \geqslant 0$ and each $i \in \mathcal{V}$;
- **internal boundedness**: all loop filter states (if any) are bounded in forward time.

The constraint interval $\mathcal{I}$ used in this definition characterizes the desired range of frequencies for the oscillators. Choosing an appropriate interval $\mathcal{I}$ in the design is thus useful for preventing the oscillators from moving too fast, too slow, or reversing direction.

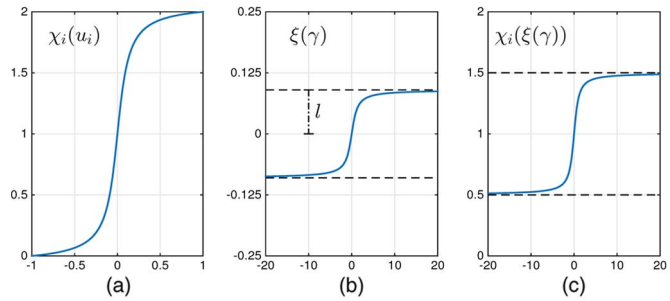

Fig. 2. Examples of $\chi_i(\cdot)$ and $\xi(\cdot)$ such that $\chi_i(\xi(\cdot)) \in [.5, 1.5]$.

A. Base Oscillator and Phase Comparator

In common models of controlled analog oscillators, the instantaneous frequency is some uncertain monotonic nonlinear function of the control input. For example, the graph of this function is the "tuning curve" seen on data sheets of many voltage-controlled oscillatorVCOs, where it is understood that this curve is typical rather than exact. Motivated by such models, we assign an uncertain *frequency function* χ_i to the base oscillator in each vertex i, where $\chi_i : \mathcal{U} \to \mathbb{R}$ is a strictly increasing C^1 function on a known open interval domain $\mathcal{U} \subset \mathbb{R}$; see Fig. 2(a). The angular velocity of the phase of the oscillator at time t (that is, its instantaneous frequency) is then given by $\chi_i(u_i(t))$, where $u_i(\cdot)$ is a $\mathcal{U}$-valued control signal. Hence, our model for the base oscillator is the differential equation

$$\dot{\varphi}_i = \chi_i(u_i). \tag{4}$$

In this oscillator model, the oscillator stops whenever $\chi_i(u_i) = 0$ and reverses direction whenever $\chi_i(u_i)$ changes sign. However, an oscillator need not admit such behavior, as the image $\chi_i(\mathcal{U})$ need not contain zero.

As we see from the model (4), the base oscillators are nonlinear and heterogeneous. In addition, we do not need precise knowledge of the frequency functions χ_i to complete our design and guarantee almost-global synchronization. In fact, as we will see when we list our assumptions in Section III-E, all we need to know about the functions χ_i is that they are C^1 with positive derivatives on $\mathcal{U}$, and that the intersection of their images $\chi_i(\mathcal{U})$ is nonempty.

The phase comparator in vertex i calculates a linear combination of functions of phase differences to produce a phase error e_i

$$e_i(\varphi) = \sum_{(j,k)\in\mathcal{N}_i} a_k f(\varphi_j - \varphi_i) \tag{5}$$

where the constants a_k are positive edge weights and $f : \mathbb{T} \to \mathbb{R}$ is the *phase coupling function*. For example, the coupling function used in many classical PLL designs is the sine function $f = \sin$. Alternatively, one can build other coupling functions f by cascading a sawtooth phase comparator [31] and a nonlinear component that provides the f-shape or by directly synthesizing a nonlinear phase comparator [32].

B. Example: Kuramoto Model

Suppose that the frequency function χ_i for each base oscillator i has the simple affine form $\chi_i(u_i) = \omega_i + u_i$, where the constant $\omega_i \in \mathbb{R}$ represents the nominal oscillator frequency. Suppose further that the phase coupling function is the sine function $f = \sin$ and that all loop filters are constant unity gains so that $u_i \equiv_i$. Then, the controlled phase equation becomes

$$\dot{\varphi}_i = \omega_i + \sum_{(j,k)\in\mathcal{N}_i} a_k \sin(\varphi_j - \varphi_i). \tag{6}$$

This model of a network of coupled oscillators has been studied extensively, and we refer the reader to the survey paper [33]. In particular, if the graph $\mathbb{G}$ is complete, and if all edge weights a_k are the same, then this is the famous Kuramoto model of coupled oscillators [34].

The oscillator network characterized by the dynamics in (6) fails to meet the design goal of Definition 1. Indeed, the existence of a synchronized trajectory for the model (6) where $\delta\varphi \equiv 0$ implies that the nominal frequencies ω_i are all identical. If these frequencies were known precisely, then we could simply cancel them out via control by setting $u_i = e_i + \omega^\star - \omega_i$ to obtain a model of the form (6) where $\omega_i = \omega^\star$ for all $i \in \mathcal{V}$. However, even in this case of identical frequencies, almost-global synchronization has been proved only for special classes of connected graphs, such as complete graphs [35] or trees [33]. Instead, we are interested in oscillators having unknown heterogeneous frequencies on arbitrary connected graphs. In this case, one can choose sufficiently large edge weights a_k to guarantee "practical" phase synchronization where $\delta\varphi$ becomes small, provided it does not start off too large [33]. However, choosing large edge weights makes it less likely that the frequencies $\dot{\varphi}_i$ will be constrained to a desired interval $\mathcal{I}$ during the transient. In any case, we see that we must depart from this standard model (6) to meet the design goal of Definition 1, and we do so by choosing a nonsinusoidal coupling function f in (5) and a nonlinear dynamic loop filter.

C. Toward Synchronization: A Hamiltonian System

The loop filter in vertex i produces the control signal u_i from the phase error e_i. It is well known that introducing the integral action into the loop filter can compensate offset mismatches for networks of heterogeneous oscillators [19], [21]–[23], [25], [30]. Thus, as a first attempt at achieving almost-global synchronization of the oscillator network, we simply make the loop filter a scaled integrator

$$\dot{\gamma}_i = c_i e_i(\varphi) \tag{7}$$
$$u_i = \zeta(\gamma_i) \tag{8}$$

where $\gamma_i(\cdot)$ is the real-valued internal filter state, c_i is a positive parameter, and $\zeta : \mathbb{R} \to \mathcal{U}$ is a scaling function which squeezes the value of γ_i into the domain $\mathcal{U}$ of the frequency function χ_i. As shown in Fig. 2, we can choose $\zeta(\mathbb{R})$ to be a strict subset of $\mathcal{U}$, which can help us achieve the desired frequency constraint $\dot{\varphi}_i(t) \in \mathcal{I}$. For illustration purposes, in our simulations, we will use

$$\chi_i(u) = \frac{\operatorname{atan}(\alpha u)}{\operatorname{atan}(\alpha)} + 1 \quad \text{and} \quad \zeta(\gamma) = l\frac{2}{\pi}\operatorname{atan}(\gamma) \tag{9}$$

with $\alpha = 10$, $l = \chi_i^{-1}(1.5)$, and $\mathcal{U} = (-1, 1)$. Notice that the specific choice of l makes $\chi_i(\zeta(\gamma)) \in [.5, 1.5] \subset \chi_i(\mathcal{U}) = [0, 2]$.

We do not assume that the oscillators have access to the global time variable t. As a result, the differential dt used in

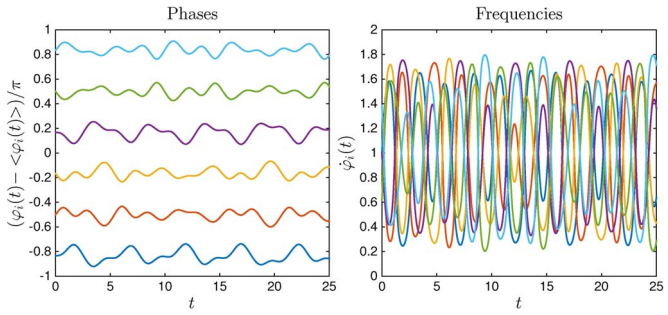

Fig. 3. Hamiltonian oscillations with $f = \sin$.

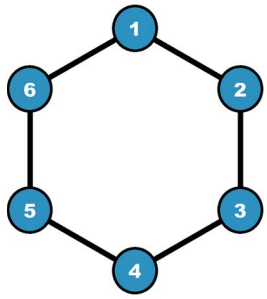

Fig. 4. Six-node graph, ring topology.

the construction of $d\gamma_i/dt$ in (7) is unknown, and we account for this by assuming that the positive constant c_i is unknown.

The system resulting from (4) and (7) and (8) is

$$\dot{\varphi}_i = \chi_i\left(\zeta(\gamma_i)\right) \tag{10}$$
$$\dot{\gamma}_i = c_i e_i(\varphi) \tag{11}$$

where e_i is the phase error in (5). The first thing we notice about this system (10), (11) is that it admits a synchronized solution at any frequency $\omega^\star \in \mathbb{R}$ which belongs to the image of each function $\chi_i \circ \zeta$. Indeed, choose any initial states such that $\delta\varphi(0) = 0$ and $\chi_i(\zeta(\gamma_i(0))) = \omega^\star$ for each $i \in \mathcal{V}$; then $\dot{\varphi}_i \equiv \omega^\star$ and $\dot{\gamma}_i \equiv 0$ for every $i \in \mathcal{V}$, which implies $\delta\varphi \equiv 0$. However, solutions starting from other initial conditions will not converge to such synchronized trajectories, which means this system still fails to meet the design goal of Definition 1. We illustrate the lack of convergence in Fig. 3, where we show the evolution of the frequencies and phases of six oscillators interconnected in a ring topology according to Fig. 4, with $a_k = 1\ \forall k$, $f = \sin$, and χ_i and ζ given by (9), with $\alpha = 10$ and $l = 1$.[2]

The second thing we notice about the system (10), (11) is that it is a Hamiltonian system with position variables φ_i and momentum variables γ_i/c_i. Indeed, assuming the phase coupling function f is odd, the n-vector of phase errors e_i is the negative gradient of a potential function of the phase vector φ (as we will show in Section IV-A). Furthermore, each function $(\chi_i \circ \zeta)/c_i$, being a scalar function of a scalar variable, is trivially the gradient of a potential function of its argument γ_i. The sum of these potential functions is a Hamiltonian associated with the dynamics (10)–(11). Moreover, as we will see in Section IV-A, if we let the position variables be the phases φ_i measured relative to an appropriate rotating frame, then the system is still Hamiltonian, but now the Hamiltonian is proper and non-

[2]The expression $\langle\varphi_i(t)\rangle$ that appears in the figures of this paper is used for representation only. It amounts to the coordinate-dependent average, that is, $\langle\varphi_i(t)\rangle = (1/n)\sum_{i\in\mathcal{V}} \varphi_i(t)$, when the phases $\varphi_i(t)$ represent values in $\mathbb{R}$.

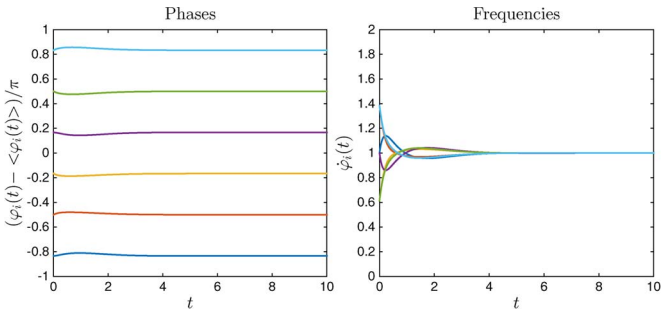

Fig. 5. Frequency synchronization without phase consensus.

negative and is thus a Lyapunov function candidate. If we can guarantee that synchronized trajectories represent the only local minima of this Lyapunov function, then we can perturb these Hamiltonian dynamics with dissipation terms in the controller to achieve almost-global synchronization. This is the control design strategy we will pursue in this paper.

D. PI Loop Filter: A Perturbed Hamiltonian System

We propose two different perturbed Hamiltonian systems in this paper—the first now and the second later on in Section III-F. For our first perturbation, we add a proportional term to the integral control (8), resulting in a proportional-integral (PI) loop filter of the form

$$\dot{\gamma}_i = c_i e_i(\varphi) \tag{12}$$
$$u_i = \zeta\left(e_i(\varphi) + \gamma_i\right). \tag{13}$$

Such a loop filter (without our nonlinear scaling function ζ) can be found in classical PLL designs [30] as well as in various coupled oscillator systems [23], [25]. More generally, the error term e_i in (13) can be replaced with a scaled error term $\kappa_i e_i$, where the "proportional gain" κ_i is a positive constant (or even a positive function of γ_i), with virtually no change in the convergence proof. We have left this gain κ_i out of the analysis to simplify notation, but the flexibility it adds will be important for tuning the performance of the system. We might also introduce a corresponding "integral gain," but for the analysis, this can be absorbed into the constant c_i.

To summarize, each controlled oscillator in the network has second-order dynamics of the form

$$\dot{\varphi}_i = \chi_i\left(\zeta\left(e_i(\varphi) + \gamma_i\right)\right) \tag{14}$$
$$\dot{\gamma}_i = c_i e_i(\varphi) \tag{15}$$

with

$$e_i(\varphi) = \sum_{(j,k)\in\mathcal{N}_i} a_k f(\varphi_j - \varphi_i). \tag{16}$$

The state space of each such oscillator is the cylinder $\mathbb{T} \times \mathbb{R}$. The system (14)–(16) has the same structure as [22] in the sense that it uses the offset error information to control θ_i and γ_i. In fact, it is easy to see that the linearization of (14)–(16) around an orbit is equivalent to a continuous time version of the algorithm proposed in [22].

Fig. 5 shows the same setup as in Fig. 3 but using (14)–(16) instead of the Hamiltonian system (10)–(11). Although the system converges to a phase-locked orbit, the phases do not reach

phase consensus. It is possible to show that this property is generic within a neighborhood of $a_k = 1$. Thus, there is a set of initial conditions with positive measure so that trajectories starting within this set achieve frequency synchronization but not asymptotic phase synchronization. In this paper, we will solve the lack of phase consensus by choosing a nonsinusoidal f.

We next present conditions under which this oscillator system exhibits almost-global synchronization within a given interval $\mathcal{I}$.

E. Assumptions and Main Result

We assume that each vertex knows its neighbors in the graph $\mathbb{G}$ (as they need to exchange phase information), but otherwise the graph is unknown. However, we do assume the following:

A1) the graph $\mathbb{G}$ is connected, and there exists a known upper bound on the number n of vertices in $\mathbb{G}$.

The frequency functions χ_i of the base oscillators are uncertain; we merely assume that they satisfy the following:

A2) the frequency functions $\chi_i : \mathcal{U} \to \mathbb{R}$ are all C^1 with positive derivatives $\chi_i' : \mathcal{U} \to (0, \infty)$, and have a common nonempty frequency range, i.e.,

$$\bigcap_{i \in \mathcal{V}} \chi_i(\mathcal{U}) \neq \varnothing. \tag{17}$$

It is clear from the oscillator model (4) that (17) is necessary for the existence of phase trajectories having synchronized frequencies. This condition (17) implies the existence of some common interval of possible base oscillator frequencies and, thus, places an inherent limit on the extent to which these oscillators can differ from each other. Indeed, if one oscillator can only produce frequencies in the kilohertz range and another only in the megahertz range, then there is no possibility of synchronization.

We next assume that our loop filter scaling function ζ satisfies:

A3) the scaling function $\zeta : \mathbb{R} \to \mathcal{U}$ is C^1 with positive derivative $\zeta' : \mathbb{R} \to (0, \infty)$, and is such that

$$\bigcap_{i \in \mathcal{V}} \chi_i \left(\zeta(\mathbb{R}) \right) \neq \varnothing \tag{18}$$

$$\bigcup_{i \in \mathcal{V}} \chi_i \left(\zeta(\mathbb{R}) \right) \subset \mathcal{I} \tag{19}$$

where $\mathcal{I}$ is the constraint interval from Definition 1.

It is clear from (4) that (19) constrains the frequencies $\dot{\varphi}_i$ to the interval $\mathcal{I}$ as required by the design goal in Definition 1. If $\mathcal{I}$ is large enough to contain the union of the images $\chi_i(\mathcal{U})$, then we can always satisfy assumption **A3**) by choosing the scaling function ζ to be a diffeomorphism onto $\mathcal{U}$ [so that (17) and (18) are the same]. However, if $\mathcal{I}$ is not that large, then assumption **A3**) states that we have found a solution to the problem of designing ζ to satisfy both (18) and (19) based on some *a priori* knowledge about the set of possible frequency functions χ_i. Such a design problem could very well have no solution if $\mathcal{I}$ is too small.

We let $f' : \mathbb{T} \to \mathbb{R}$ denote the derivative of the phase coupling function f in the direction of the unit vector field $\hat{\imath}$. We make two assumptions on this function f:

A4) the phase coupling function $f : \mathbb{T} \to \mathbb{R}$ is C^1 and odd, that is, $f(-\theta) = -f(\theta)$ for all $\theta \in \mathbb{T}$;

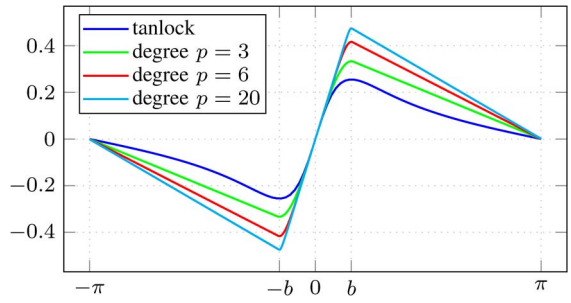

Fig. 6. Examples of phase-coupling functions f when $b = 0.5$.

A5) there is a constant $b \in (0, \pi/(n-1)]$ such that $f'(\theta) > 0$ whenever $\cos(\theta) > \cos(b)$ and $f'(\theta) < 0$ whenever $\cos(\theta) < \cos(b)$, for any $\theta \in \mathbb{T}$.

Assumptions A4) and A5) also appeared in [36] and [37] and play an important role in the convergence analysis: A4) allows the interpretation of (4) and (7) and (8) as a Hamiltonian system, while **A5**) is needed to guarantee convergence to the desired solution.

Note that to choose such a parameter b, we must use our assumed knowledge in (**A1**) of a known upper bound on n. Examples of functions f which satisfy assumptions **A4**)–**A5**) are shown in Fig. 6 for $b = 0.5$. The first example is given by the C^ω formula

$$f(\theta) = [1 - \cos(b)] \, \frac{\sin(\theta)}{1 - \cos(b)\cos(\theta)}. \tag{20}$$

This function is related to the characteristic of certain "tanlock" phase comparators [30], and it generates the sinusoidal coupling $f = \sin$ when $b = \pi/2$. The other examples are C^1 and piecewise polynomial of various degrees $p \geqslant 1$, each having a derivative given by $f'(\theta) = 1 - (|\theta|/b)^{p-1}$ on a certain arc containing $[-b, b]$ and a constant derivative on the complement of $[-b, b]$. All of these examples are normalized to have a unit derivative at zero, which means they should result in similar performance for small deviations around a stable synchronized trajectory. When b is small (which we require when n is large), the magnitude of the derivative of the tanlock function is small on the arc $[b, \pi]$ when compared to the magnitude of the derivatives of the piecewise-polynomial functions. As a result, the piecewise-polynomial functions might provide faster convergence to a synchronized state when some initial phase differences are greater than b (due to their larger gains for large phase differences). Note that it is *not* the case that the slope $f'(0)$ must get large as b gets small—ours is not a high-gain solution. In fact, because the edge weights a_k can be arbitrarily small, our solution includes low-gain designs.

The final assumption is on the choice of the edge weights a_k:

A6) each edge weight a_k is chosen at random from a continuous probability distribution on the interval $(0, \infty)$.

This assumption allows us to state that with probability one, we avoid an unknown zero-measure set of bad edge weight vectors $a = [a_1 \ldots a_m]^T \in \mathbb{R}^m$ for which our stability analysis does not guarantee convergence.

Theorem 2: Assume **A1**)–**A6**). Then, with probability one in the selection of edge weights in (**A6**), the network of oscillators with vertex dynamics (14)–(16) achieves almost-global synchronization within $\mathcal{I}$.

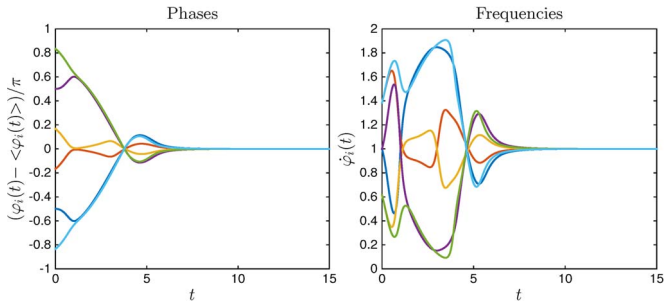

Fig. 7. Decaying oscillations with tanlock f.

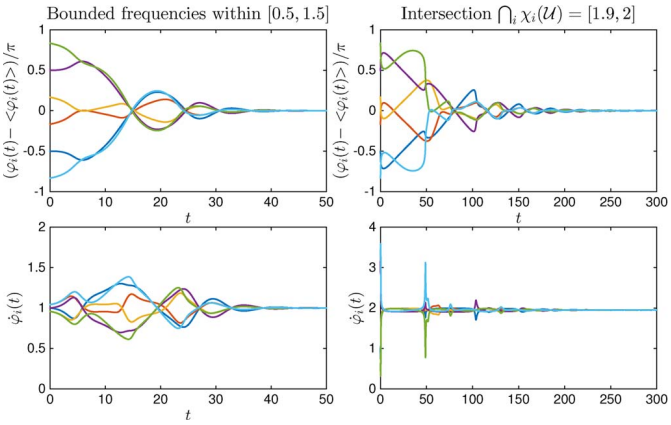

Fig. 8. Additional properties of controllers.

Note that when $n \geqslant 4$, assumption **A5**) rules out the sinusoidal phase-coupling function $f = \sin$. In fact, the requirement $b \leqslant \pi/(n-1)$ is within a factor of two of being necessary. Indeed, one can show that for a oscillator network of size n and ring topology, the uniformly distributed phase-locked orbit with $f = \sin$, illustrated in Fig. 5 for $n = 6$, is stable for all $b > (2\pi/n)$. In contrast, Fig. 7 shows that when substituting sin with the tanlock function (20) with $b = \pi/5$, the same initial condition now converges to the desired orbit as predicted by Theorem 2.

Finally, we illustrate two interesting characteristics of our controllers in Fig. 8. In the left column of Fig. 8, we show how by setting $l = \chi_i^{-1}(1.5)$ as in Fig. 2, we are able to constrain the oscillator frequencies to lie within (0.5, 1.5). In the right column, we change the range of χ_i to be $\chi_1(\mathcal{U}) = \chi_3(\mathcal{U}) = \chi_5(\mathcal{U}) = (0, 2)$ and $\chi_2(\mathcal{U}) = \chi_4(\mathcal{U}) = \chi_6(\mathcal{U}) = (1.9, 3.9)$. We can see that despite the very narrow intersection of frequency ranges, the oscillators still synchronize in frequency and phase.

We will prove Theorem 2 in Section IV. In this proof, we first construct a Lyapunov function for the system, and then apply the Krasovskii–LaSalle invariance theorem to show that all trajectories converge to a certain invariant subset $\mathcal{M}$ of the state space $\mathbb{T}^n \times \mathbb{R}^n$. We then determine the structure of this set $\mathcal{M}$, showing first that it is the disjoint union of isolated embeddings of the cylinder $\mathbb{T} \times \mathbb{R}$. We next show that the state space admits a foliation into invariant $(2n-1)$-dimensional submanifolds, and that the intersection of each leaf of this foliation with the set $\mathcal{M}$ is the disjoint union of isolated embeddings of the circle $\mathbb{T}$ (as conceptualized in Fig. 9). Each such circle represents a periodic trajectory with a constant synchronized frequency $\omega^\star \in \mathcal{I}$ (so that $\dot{\varphi}_i \equiv \omega^\star$). One of the cylinders of the set $\mathcal{M}$ is good, in that all of the periodic trajectories on this cylinder are also synchronized in phase (so that $\delta\varphi \equiv 0$). The remaining cylinders of $\mathcal{M}$ (if any) are bad, in that all of the periodic trajectories on these cylinders are out of phase. Finally, using a local linearization analysis, we show that the phase-synchronized trajectories are exponentially stable (relative to each leaf of the foliation), whereas the out-of-phase trajectories are exponentially unstable. Because we show that these periodic trajectories are *isolated* on each leaf (a key step in the proof), we conclude that almost all trajectories achieve asymptotic synchronization in both frequency and phase.

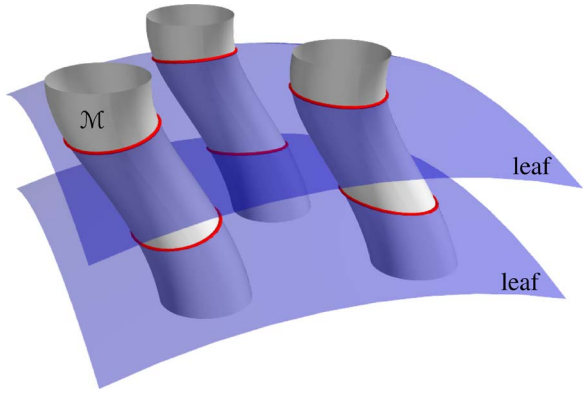

Fig. 9. Invariant set $\mathcal{M}$ (shown in gray) is a collection of isolated cylinders. The intersection of each invariant leaf of the foliation (shown in blue) with $\mathcal{M}$ is a collection of isolated circles (shown in red).

F. Dual Controller: A Different Perturbed Hamiltonian System

The approach we take in the controller design in (14)–(16) is to perturb the Hamiltonian system (10), (11) by adding a dissipation term to the dynamics of each position variable. An alternative, dual approach is to add a dissipation term to the dynamics of each momentum variable. We will do this by including a second comparator in addition to the phase comparator, that is, by introducing a second set of error signals z_i in addition to the phase errors e_i in (5). The resulting controller is more complex, but further analysis might reveal that it has performance advantages over the controller (14)–(16).

For this dual controller, each pair of neighboring vertices agrees on an orientation of the edge connecting them. Thus, each vertex i can partition its neighbor set as $\mathcal{N}_i = \mathcal{N}_i^+ \cup \mathcal{N}_i^-$, where $(j,k) \in \mathcal{N}_i^+$ when i is the head of the edge $k = \{i, j\}$ and $(j,k) \in \mathcal{N}_i^-$ when i is the tail of the edge k. Furthermore, we make an additional assumption on the frequency functions χ_i of the base oscillators:

A7) the interval $\mathcal{U}$ and the intervals $\chi_i(\mathcal{U})$ for each $i \in \mathcal{V}$ contain only positive real numbers.

In other words, we assume that the graph of each $\chi_i(\cdot)$ lies completely in the first quadrant, which is true for many analog oscillators. This assumption guarantees that the functions ζ and χ_i take on only positive values. Consequently, for each ordered pair of vertices ij, we can define the ratio

$$\rho_{ij}(\gamma_i, \gamma_j) = \frac{\zeta(\gamma_j)\chi_i(\zeta(\gamma_i))}{\zeta(\gamma_i)\chi_j(\zeta(\gamma_j))} > 0. \tag{21}$$

Using (10), that is, using the base oscillator model (14), together with the integrator loop filter (7), (8), we can calculate

(21) as

$$\rho_{ij}(\gamma_i,\gamma_j)=\frac{\zeta(\gamma_j)}{\zeta(\gamma_i)}\left[\frac{d\varphi_j}{d\varphi_i}\right]^{-1}. \tag{22}$$

We then define a new error signal z_i for vertex i as

$$\begin{aligned} z_i(\gamma)=&\sum_{(j,k)\in\mathcal{N}_i^+} d_k\left[\zeta(\gamma_j)-\rho_{ij}(\gamma_i,\gamma_j)\zeta(\gamma_i)\right]\\ &+\sum_{(j,k)\in\mathcal{N}_i^-} d_k\left[\rho_{ij}^{-1}(\gamma_i,\gamma_j)\zeta(\gamma_j)-\zeta(\gamma_i)\right] \end{aligned} \tag{23}$$

where $\gamma=[\gamma_1\ \dots\ \gamma_n]^T\in\mathbb{R}^n$ is the vector of loop filter states and the constants d_k are an additional set of positive edge weights. For vertex i to compute this error variable z_i, it must receive the signal $\zeta(\gamma_j)$ from each of its neighbors. Also, we see from (22) that it must calculate the derivative of each neighbor's phase φ_j with respect to its own phase φ_i, a calculation which does not require knowledge of the global time variable t.

Using these new error signals z_i, we define the dual perturbed Hamiltonian system as

$$\dot{\varphi}_i=\chi_i(\zeta(\gamma_i)) \tag{24}$$
$$\dot{\gamma}_i=c_ie_i(\varphi)+c_iz_i(\gamma). \tag{25}$$

Thus, we have retained the simple integrator loop filter in (7) and (8), but have changed its input from e_i to the sum e_i+z_i. This amounts to modifying Fig. 1 by putting a "γ-comparator" in parallel with the phase comparator.

Although at first sight the physical interpretation of z_i is obscured by the implementation details, substituting (21) and (24) into (23) gives

$$\begin{aligned} z_i(\gamma)&=\sum_{(j,k)\in\mathcal{N}_i}\eta_k(\gamma)\left[\chi_j(\zeta(\gamma_j))-\chi_i(\zeta(\gamma_i))\right]\\ &=\sum_{(j,k)\in\mathcal{N}_i}\eta_k(\gamma)\left[\dot{\varphi}_j-\dot{\varphi}_i\right] \end{aligned} \tag{26}$$

with

$$\eta_k(\gamma)=d_k\frac{\zeta(\gamma_j)}{\chi_j\left(\zeta(\gamma_j)\right)}\ \text{where } j \text{ is the tail of edge } k \tag{27}$$

for each $k\in\mathcal{E}$. Therefore, (23) can be interpreted as an indirect estimate of the frequency mismatch (26) between oscillator i and its neighbors. As we will see in the proof of the following theorem in Section V, this frequency's error terms z_i are the right perturbation that need to be added to the dynamics of the momentum variables to guarantee the dissipation of the Hamiltonian energy.

Theorem 3: Assume **A1**)–**A7**). Then, with probability one in the selection of edge weights in **A6**), the network of oscillators with vertex dynamics (23)–(25) achieves almost-global synchronization within $\mathcal{I}$.

The proof of this theorem is similar to that of Theorem 2, and we will highlight the main differences in Section V.

IV. Proof of Theorem 2

For any $p\in\mathbb{N}$, we let $\mathbf{0}_p$ and $\mathbf{1}_p$ denote the column vectors of p zeros and p ones, respectively, and we let I_p denote the $p\times p$ identity matrix. Any $\ell\times p$ matrix with integer elements will represent either an $\mathbb{R}$-linear map from $\mathbb{R}^p$ to $\mathbb{R}^\ell$ or a $\mathbb{Z}$-linear map from $\mathbb{T}^p$ to $\mathbb{T}^\ell$, depending on context. In particular, if M is an $\ell\times p$ matrix with integer elements and $t\mapsto x(t)$ is a curve in $\mathbb{T}^p$, then $t\mapsto y(t)=Mx(t)$ is a curve in $\mathbb{T}^\ell$ (with M representing a $\mathbb{Z}$-linear map) and, furthermore, $\dot{y}(t)=M\dot{x}(t)$ for all t (with M now representing an $\mathbb{R}$-linear map).

We first introduce some notation for writing the overall coupled dynamics (14)–(16) in a compact form. We define state vectors

$$\varphi=[\varphi_1\ \dots\ \varphi_n]^T\quad\in\mathbb{T}^n \tag{28}$$
$$\gamma=[\gamma_1\ \dots\ \gamma_n]^T\quad\in\mathbb{R}^n \tag{29}$$

along with the following diagonal matrices:

$$A=\operatorname{diag}\{a_1,\dots,a_m\}\quad\in\mathbb{R}^{m\times m} \tag{30}$$
$$C=\operatorname{diag}\{c_1,\dots,c_n\}\quad\in\mathbb{R}^{n\times n}. \tag{31}$$

For convenience, we define $\sigma_i=\chi_i\circ\zeta$ for each i, and we note from assumptions **A2**) and **A3**) that each σ_i is C^1 with a positive derivative. We next define mappings $F:\mathbb{T}^m\to\mathbb{R}^m$ and $\Sigma:\mathbb{R}^n\to\mathbb{R}^n$ by

$$F(\theta)=[f(\theta_1)\ \dots\ f(\theta_m)]^T\ \in\mathbb{R}^m \tag{32}$$
$$\Sigma(y)=[\sigma_1(y_1)\ \dots\ \sigma_n(y_n)]^T\ \in\mathbb{R}^n \tag{33}$$

where $\theta=[\theta_1\ \dots\ \theta_m]^T\in\mathbb{T}^m$ and $y=[y_1\ \dots\ y_n]^T\in\mathbb{R}^n$. Note that Σ is a C^1 diffeomorphism onto its image $\Sigma(\mathbb{R}^n)$. Finally, we let $B\in\{-1,0,1\}^{n\times m}$ be an oriented incidence matrix for the graph $\mathbb{G}$. Using the fact from **A4**) that f is odd, we can write the dynamics (14)–(16) as

$$\dot{\varphi}=\Sigma(-BAF(B^T\varphi)+\gamma) \tag{34}$$
$$\dot{\gamma}=-CBAF(B^T\varphi). \tag{35}$$

For convenience, we define $e:\mathbb{T}^n\to\mathbb{R}^n$ by

$$e(\varphi)=[e_1(\varphi)\ \dots\ e_n(\varphi)]^T=BAF(B^T\varphi) \tag{36}$$

which enables us to write (34) and (35) as

$$\dot{\varphi}=\Sigma(e(\varphi)+\gamma) \tag{37}$$
$$\dot{\gamma}=Ce(\varphi). \tag{38}$$

Note that $1_n^Te\equiv 0$ because $1_n^TB=0$ (a property of any oriented incidence matrix). This property also implies $e(\varphi)=e(\varphi+1_n\theta)$ for any $\varphi\in\mathbb{T}^n$ and any $\theta\in\mathbb{T}$.

A. Global Lyapunov Function

In this section, we construct a Lyapunov function for the system (37), (38), which is the Hamiltonian we described in Section III-C for the system (10), (11).

Since f is odd from **A4**), the integral of the 1-form $f\cdot\langle\partial,\cdot\rangle$ around any smooth closed curve in $\mathbb{T}$ is zero. Thus, this 1-form is the differential of a smooth function $\Psi:\mathbb{T}\to\mathbb{R}$, which is unique up to an additive constant (which we choose so that the minimum value of Ψ on $\mathbb{T}$ is zero). Therefore, $d/dt(\Psi\circ x)\equiv f(x)\dot{x}$ for any curve $x:\mathbb{R}\to\mathbb{T}$. We then define $V:\mathbb{T}^m\to[0,\infty)$ as the sum

$$V(\theta)=\sum_{k\in\mathcal{E}}a_k\Psi(\theta_k) \tag{39}$$

where $\theta=[\theta_1\dots\theta_m]^T\in\mathbb{T}^m$. It follows that:

$$\frac{d}{dt}V(B^T\varphi)=F^T(B^T\varphi)AB^T\dot{\varphi}=-e^T(\varphi)\dot{\varphi}. \tag{40}$$

From (18), there exists a frequency $\varpi \in \bigcap_i \sigma_i(\mathbb{R})$. Therefore, the function $W : \mathbb{R}^n \to [0, \infty)$ defined as

$$W(\gamma) = \sum_{i \in \mathcal{V}} \frac{1}{c_i} \int_{\sigma_i^- 1(\varpi)}^{\gamma_i} [\sigma_i(s) - \varpi]\, ds \tag{41}$$

is proper (because σ_i is increasing) and has a derivative given by

$$\frac{d}{dt} W(\gamma) = \left[\Sigma^T(\gamma) - \varpi \mathbf{1}_n^T\right] C^{-1} \dot{\gamma}. \tag{42}$$

We now obtain a Lyapunov function by adding (39) and (41): we define $U : \mathbb{T}^n \times \mathbb{R}^n \to [0, \infty)$ by

$$U(\varphi, \gamma) = V(B^T \varphi) + W(\gamma) \tag{43}$$

which is a proper function on $\mathbb{T}^n \times \mathbb{R}^n$. Because $\mathbf{1}_n^T e \equiv 0$, the derivative of (43) along the trajectories of (37) and (38) is

$$\begin{aligned} \dot{U} &= -e^T(\varphi) \Sigma\left(e(\varphi) + \gamma\right) + \Sigma^T(\gamma) e(\varphi) \\ &= -e^T(\varphi) \int_0^1 \Sigma'\left(e(\varphi) s + \gamma\right) ds \cdot e(\varphi) \end{aligned} \tag{44}$$

where $\Sigma'(\cdot)$ denotes the diagonal Jacobian matrix

$$\Sigma'(\gamma) = \operatorname{diag}\left\{\sigma_1'(\gamma_1), \ldots, \sigma_n'(\gamma_n)\right\}. \tag{45}$$

Because $\Sigma'(\cdot)$ is positive definite, we have $\dot{U} \leqslant 0$ and $\dot{U} = 0$ if and only if $e(\varphi) = 0$. It follows from the Krasovskii–LaSalle invariance theorem that all trajectories of the system (37), (38) converge to the largest invariant set $\mathcal{M}$ contained within the set $\Phi \times \mathbb{R}^n$, where $\Phi \subset \mathbb{T}^n$ denotes the set

$$\Phi = e^{-1}\left(\{0\}\right) = \left\{\varphi \in \mathbb{T}^n : BAF(B^T \varphi) = 0\right\}. \tag{46}$$

Note that because $B^T \mathbf{1}_n = 0$, this set Φ has the symmetry property $\Phi = \Phi + \mathbf{1}_n \mathbb{T}$. Also, it follows from **A4**) that $F(0) = 0$, which means Φ contains all points of the form $\mathbf{1}_n \theta$ for $\theta \in \mathbb{T}$. The next step in the proof is to investigate the structure of this set $\mathcal{M}$.

B. Structure of the Set $\mathcal{M}$

In this section, we show that the largest invariant set $\mathcal{M}$ contained within the set $\Phi \times \mathbb{R}^n$ is $\mathcal{M} = \Phi \times \Gamma$, where Φ in (46) is the zero set of e, and $\Gamma \subset \mathbb{R}^n$ is the set

$$\Gamma = \left\{\gamma \in \mathbb{R}^n : B^T \Sigma(\gamma) = 0\right\}. \tag{47}$$

We begin by exploring the structure of these sets Φ and Γ. First, we show that Φ is the disjoint union of isolated embeddings of the circle $\mathbb{T}$. Next, we show that $\Gamma = \alpha(\mathbb{R})$, where $\alpha : \mathbb{R} \to \mathbb{R}^n$ is a C^1 curve in $\mathbb{R}^n$. Moreover, if we let $q \in \mathbb{R}^n$ denote the unit vector in the direction of $C^{-1}\mathbf{1}_n$, then this curve α is such that $q^T \alpha(\cdot)$ is the identity map on $\mathbb{R}$. Finally, we show that $\mathcal{M} = \Phi \times \Gamma$, that is, that $\mathcal{M}$ is the disjoint union of isolated embeddings of the cylinder, as illustrated in Fig. 9.

Structure of Φ: We partition $\mathbb{T}^n$ using the following matrices:

$$R = \begin{bmatrix} \mathbf{0}_{n-1}^T \\ I_{n-1} \end{bmatrix} \quad \in \{0, 1\}^{n \times (n-1)} \tag{48}$$

$$S = \begin{bmatrix} -\mathbf{1}_{n-1}^T \\ I_{n-1} \end{bmatrix} \quad \in \{-1, 0, 1\}^{n \times (n-1)}. \tag{49}$$

Clearly, the state φ satisfies the identity

$$\varphi = \mathbf{1}_n \varphi_1 + R S^T \varphi \tag{50}$$

which defines the direct sum $\mathbb{T}^n = \mathbf{1}_n \mathbb{T} \oplus R\mathbb{T}^{n-1}$. Here, the first summand represents the first component angle and the second one represents the remaining angles measured relative to the first. Note that $S^T R = I_{n-1}$, that $S^T \mathbf{1}_n = 0$, and that $B^T = B^T R S^T$. Also, because $\mathbb{G}$ is connected from **A1**), we have $\operatorname{rank}(B) = n-1$ and, thus, the columns of $B^T R$ are independent.

Because $\varphi \in \Phi$ if and only if $RS^T \varphi \in \Phi$, it follows from (50) that $\Phi = RS^T \Phi + \mathbf{1}_n \mathbb{T}$. It also follows that for any $\mu \in \mathbb{T}^{n-1}$, we have $\mu \in S^T \Phi$ if and only if $R\mu \in \Phi$, that is, if and only if $e(R\mu) = 0$. We next show that the points in the set $S^T \Phi$ are isolated, which implies that Φ is the disjoint union of isolated embeddings of the circle $\mathbb{T}$.

Using the above partition of $\mathbb{T}^n$, we define two symmetric matrix functions $L : \mathbb{T}^{n-1} \to \mathbb{R}^{n \times n}$ and $L^\flat : \mathbb{T}^{n-1} \to \mathbb{R}^{(n-1) \times (n-1)}$ by

$$L(\mu) = BAF'(B^T R \mu) B^T \quad \text{and} \quad L^\flat(\mu) = R^T L(\mu) R \tag{51}$$

for $\mu \in \mathbb{T}^{n-1}$, where $F'(\cdot)$ denotes the diagonal Jacobian matrix

$$F'(\theta) = \operatorname{diag}\left\{f'(\theta_1), \ldots, f'(\theta_m)\right\} \tag{52}$$

with $\theta = [\theta_1 \ldots \theta_m]^T \in \mathbb{T}^m$. Here, $L(\mu)$ represents a weighted Laplacian matrix for the graph $\mathbb{G}$ in which the weights can have positive, negative, or zero values. Also, because $B = SR^T B$, we have

$$L(\mu) R = S L^\flat(\mu) \quad \text{and} \quad L(\mu) = S L^\flat(\mu) S^T \tag{53}$$

for all $\mu \in \mathbb{T}^{n-1}$. Note that $L(\mu)$ is congruent to the block-diagonal matrix $\operatorname{diag}\{0, L^\flat(\mu)\}$. The proof of the following theorem is in Appendix A:

Theorem 4: There is a closed set $\mathcal{Z} \subset \mathbb{R}^m$ having a zero Lebesgue measure such that if $a = [a_1 \ldots a_m]^T \notin \mathcal{Z}$, then the matrix $L^\flat(\mu)$ in (51) is invertible for all $\mu \in S^T \Phi$.

Corollary 5: If $a \notin \mathcal{Z}$, then the points in $S^T \Phi$ are isolated.

Proof: Define the mapping $P : \mathbb{T}^{n-1} \to \mathbb{R}^{n-1}$ by setting $P(\mu) = R^T BAF(B^T R \mu)$ so that $P^{-1}(\{0\}) = S^T \Phi$. The Jacobian matrix for P is just $L^\flat(\mu)$ which, by Theorem 4, is invertible for all $\mu \in S^T \Phi$. The result follows from the inverse function theorem. ■

We do not provide a method for computing the set $\mathcal{Z}$ of bad edge weight vectors, although it is clear from (46) and (51) that this set $\mathcal{Z}$ depends only on the graph $\mathbb{G}$ (through B) and the phase coupling function f (through F). Instead, we rely on the random edge weight selection in **A6**) to avoid this zero-measure set: from now on, we will assume $a \notin \mathcal{Z}$, which occurs with probability one according to **A6**).

Remark 6: Theorem 4 guarantees that the set $\mathcal{Z}$ of undesired weights a_k is nowhere dense. However, in practice, the weights a_k can take on only finitely many values due to limited machine precision, and we thus can no longer guarantee that their random selection *within this finite-precision set* will avoid the set $\mathcal{Z}$ with probability one. Nevertheless, our simulations indicate that we do indeed always avoid $\mathcal{Z}$ when choosing finite-precision weights at random. In fact, if we further assume that f is piecewise analytic, which is the case for all of the examples presented in this paper, then we can show that $\mathcal{Z}$ is a

subanalytic set and is therefore a locally finite union of embedded submanifolds of dimension at most $m-1$. This makes it highly unlikely that we will generate random weights in $\mathcal{Z}$ even when using finite precision.

Structure of Γ*:* To explore the structure of the set Γ in (47), we partition $\mathbb{R}^n$ by defining $q \in \mathbb{R}^n$ and $Q \in \mathbb{R}^{n\times(n-1)}$ as

$$q = \frac{C^{-1}\mathbf{1}_n}{\|C^{-1}\mathbf{1}_n\|} \quad \text{and} \quad Q = CS(S^TC^2S)^{-\frac{1}{2}}. \tag{54}$$

Using the fact that $\mathbf{1}_n^TS = 0$, it is straightforward to show that the $n \times n$ matrix $[q\ Q]$ is orthogonal; thus, the state γ satisfies the identity

$$\gamma = qq^T\gamma + QQ^T\gamma \tag{55}$$

which defines the direct sum $\mathbb{R}^n = q\mathbb{R} \oplus Q\mathbb{R}^{n-1}$ via orthogonal projections. We define the open interval $J \subset \mathbb{R}$ as

$$J = \bigcap_{i\in\mathcal{V}} \sigma_i(\mathbb{R}) \tag{56}$$

which is nonempty from (18). Because $s\mathbf{1}_n \in \Sigma(\mathbb{R}^n)$ for all $s \in J$, we can define the function $\beta : J \to \mathbb{R}$ as

$$\beta(s) = \sum_{i\in\mathcal{V}} q_i\sigma_i^{-1}(s) = q^T\Sigma^{-1}(s\mathbf{1}_n) \tag{57}$$

where the constants q_i are the components of the vector q. Note that each term in the sum in (57) is strictly increasing in s. Suppose $\{s_\ell\}$ is a sequence in J such that $s_\ell \to \sup J$ as $\ell \to \infty$. Then there exists $i \in \mathcal{V}$ such that $s_\ell \to \sup \sigma_i(\mathbb{R})$ as $\ell \to \infty$, which means $\sigma_i^{-1}(s_\ell) \to \infty$ as $\ell \to \infty$. Thus, $\beta(s_\ell) \to \infty$ as $\ell \to \infty$, which means $\sup \beta(J) = \infty$. Similar reasoning yields $\inf \beta(J) = -\infty$, and we conclude that β is invertible. Therefore, we can define a C^1 curve $\alpha : \mathbb{R} \to \mathbb{R}^n$ as follows:

$$\alpha(r) = \Sigma^{-1}\left(\beta^{-1}(r)\mathbf{1}_n\right) \tag{58}$$

which satisfies $q^T\alpha(r) = \beta(\beta^{-1}(r)) = r$ for all $r \in \mathbb{R}$. Because $\operatorname{rank}(B) = n-1$, it follows from (47) that $\gamma \in \Gamma$ if and only if $\Sigma(\gamma) = x\mathbf{1}_n$ for some $x \in J$, that is, if and only if

$$\gamma = \Sigma^{-1}(x\mathbf{1}_n) = \Sigma^{-1}\left(\beta^{-1}(\beta(x))\,\mathbf{1}_n\right) = \alpha\left(\beta(x)\right) \tag{59}$$

for some $x \in J$. Therefore, $\Gamma = \alpha(\beta(J)) = \alpha(\mathbb{R})$.

Our remaining task in this section is to show that $\mathcal{M} = \Phi \times \Gamma$.

Proof of $\mathcal{M} = \Phi \times \Gamma$*:* First, we calculate the derivative of $e(\varphi)$ in (36) using (37)

$$\begin{aligned}\dot{e} &= -BAF'(B^T\varphi)B^T\Sigma\left(e(\varphi)+\gamma\right)\\ &= -L(S^T\varphi)\Sigma\left(e(\varphi)+\gamma\right).\end{aligned} \tag{60}$$

We see from (37) and (38) that $\dot{\varphi} = \Sigma(\gamma)$ and $\dot{\gamma} = 0$ on the set $\Phi \times \mathbb{R}^n$, which means the second derivative $\ddot{\varphi}$ is zero

$$\begin{aligned}0 = \ddot{\varphi} &= -\Sigma'(\gamma)L(S^T\varphi)\Sigma(\gamma)\\ &= -\Sigma'(\gamma)SL^\flat(S^T\varphi)S^T\Sigma(\gamma)\end{aligned} \tag{61}$$

on $\Phi\times\mathbb{R}^n$. Now $\Sigma'(\cdot)$ in (45) is positive definite, $L^\flat(S^T\varphi)$ is invertible from Theorem 4, and S in (49) has independent columns; therefore, (61) implies $S^T\Sigma(\gamma) = 0$. Because $B^T = B^TRS^T$, this, in turn, implies $B^T\Sigma(\gamma) = 0$, and we conclude that $\mathcal{M} \subset \Phi\times\Gamma$. We observe that $\Phi\times\Gamma$ is itself invariant under the dynamics (37) and (38), and it follows that $\mathcal{M} = \Phi\times\Gamma$.

To summarize the results of this section, we have found that $(\varphi,\gamma) \in \mathcal{M}$ if and only if $e(\varphi) = 0$ and $\gamma = \alpha(r)$ for some $r \in \mathbb{R}$, in which case $r = q^T\gamma$. Furthermore, the zero set of e in (46) is $RS^T\Phi + \mathbf{1}_n\mathbb{T}$, where the points in $S^T\Phi$ are isolated.

C. Global Analysis: Frequency Synchronization

To study the synchronization properties of our system (37), (38), we first observe that $q^T\dot{\gamma} \equiv 0$, which means the state space admits a foliation whose leaves are the invariant manifolds $\mathbb{T}^n \times \Xi_r$, where

$$\Xi_r = qr + Q\mathbb{R}^{n-1} = \{\gamma \in \mathbb{R}^n : q^T\gamma = r\} \tag{62}$$

for a constant parameter $r \in \mathbb{R}$. Note that because $\Gamma = \alpha(\mathbb{R})$ and $q^T\alpha(\cdot)$ is the identity map, the intersection $\Gamma \cap \Xi_r$ is the Singleton $\{\alpha(r)\}$. Thus, the intersection of each invariant leaf $\mathbb{T}^n \times \Xi_r$ with $\mathcal{M} = \Phi \times \Gamma$ is just $\Phi \times \{\alpha(r)\}$, which we have shown to be the disjoint union of isolated embeddings of the circle $\mathbb{T}$ (depicted as red circles in Fig. 9).

We now fix $r \in \mathbb{R}$ and examine the dynamics on $\mathbb{T}^n \times \Xi_r$, noting that $\gamma \equiv qr + QQ^T\gamma$ on this invariant manifold. Now that r is fixed, we will write $\alpha_r = \alpha(r)$. Because $\alpha_r = qr + QQ^T\alpha_r$, we have

$$\gamma - \alpha_r \equiv QQ^T(\gamma - \alpha_r) \tag{63}$$

on $\mathbb{T}^n \times \Xi_r$. We next define the projected state variables

$$w_1 = S^T\varphi \in \mathbb{T}^{n-1} \quad \text{and} \quad w_2 = Q^T(\gamma - \alpha_r) \in \mathbb{R}^{n-1}. \tag{64}$$

Taking time derivatives of these variables, and using (63) and the fact that $e(\varphi) = e(Rw_1)$, we obtain

$$\dot{w}_1 = S^T\Sigma\left(e(Rw_1) + Qw_2 + \alpha_r\right) \tag{65}$$

$$\dot{w}_2 = Q^TCe(Rw_1). \tag{66}$$

This is an autonomous system in the projected states (w_1, w_2), and its equilibria are precisely all points of the form $(\mu^\star, 0)$ for vectors $\mu^\star \in S^T\Phi$. Each equilibrium represents a frequency-synchronized solution of (37) and (38) with $\dot{\varphi} \equiv \beta^{-1}(r)\mathbf{1}_n$ and $\gamma \equiv \alpha_r$. The equilibrium with $\mu^\star = 0$ represents a phase-synchronized trajectory with $\delta\varphi \equiv 0$, and all other equilibria represent out-of-phase trajectories.

Furthermore, each trajectory of the system (65), (66) converges to an equilibrium, which means each trajectory of the system (37), (38) achieves asymptotic frequency synchronization. Indeed, we have shown that all trajectories of the system (37), (38) converge to the set $\mathcal{M} = \Phi \times \Gamma$ in forward time. Therefore, γ converges to the Singleton set $\Gamma \cap \Xi_r = \{\alpha_r\}$, which means w_2 converges to zero. In addition, φ converges to the set Φ, which means w_1 converges to the set $S^T\Phi$. Corollary 5 states that points in $S^T\Phi$ are isolated, and we conclude that w_1 converges to one of these points.

In the next section, we will perform a local linearization analysis at each equilibrium of the system (65), (66) to determine its stability.

D. Local Analysis: Phase Synchronization

We compute the linear approximation of the dynamics (65), (66) at an equilibrium $(\mu^\star, 0)$ as follows:

$$\dot{w}_1 \approx -S^T\Sigma'(\alpha_r)L(\mu^\star)R(w_1 - \mu^\star) + S^T\Sigma'(\alpha_r)Qw_2 \tag{67}$$

$$\dot{w}_2 \approx -Q^TCL(\mu^\star)R(w_1 - \mu^\star) \tag{68}$$

or using (53)

$$\dot{w}_1 \approx -S^T\Sigma'(\alpha_r)SL^\flat(\mu^\star)(w_1-\mu^\star) + S^T\Sigma'(\alpha_r)Qw_2 \quad (69)$$
$$\dot{w}_2 \approx -Q^TCSL^\flat(\mu^\star)(w_1-\mu^\star). \quad (70)$$

If we define the $(n-1)\times(n-1)$ matrices

$$X = S^T\Sigma'(\alpha_r)S > 0 \quad (71)$$
$$Y = Q^TCS = (S^TC^2S)^{\frac{1}{2}} > 0 \quad (72)$$
$$Z = S^T\Sigma'(\alpha_r)Q \quad (73)$$

then we can write this approximation more compactly as

$$\dot{w}_1 \approx -XL^\flat(\mu^\star)(w_1-\mu^\star) + Zw_2 \quad (74)$$
$$\dot{w}_2 \approx -YL^\flat(\mu^\star)(w_1-\mu^\star). \quad (75)$$

Note from (54) and (72) that $Q = CSY^{-1}$ so that $S = C^{-1}QY$, which means Z in (73) satisfies

$$Y^{-1}Z = Q^TC^{-1}\Sigma'(\alpha_r)Q > 0. \quad (76)$$

Thus, the linearization (74), (75) satisfies the assumptions in the following theorem, whose proof is in [38, Theor. 7].

Theorem 7: Let $\Lambda \in \mathbb{R}^{2p\times 2p}$ be the block matrix

$$\Lambda = \begin{bmatrix} -XL & Z \\ -YL & 0 \end{bmatrix} \quad (77)$$

where $L, X, Y, Z \in \mathbb{R}^{p\times p}$ satisfy:

1) L is symmetric;
2) $X + X^T > 0$;
3) Y is symmetric and invertible;
4) $Y^{-1}Z$ is symmetric with $Y^{-1}Z \geqslant 0$.

If L has a negative eigenvalue, then Λ has an eigenvalue with a positive real part. If instead Z is invertible and $L > 0$, then Λ is Hurwitz.

We can complete the local linearization analysis by applying Theorem 7 together with the following theorem.

Theorem 8: The Laplacian $L(\mu)$ has $n-1$ positive eigenvalues for $\mu = 0$, and it has at least one negative eigenvalue for any nonzero $\mu \in S^T\Phi$.

The proof of Theorem 8, which follows from [29, Lemmas 1 and 2], relies on the properties of the phase coupling function f defined in Assumption **A5**) and the graph $\mathbb{G}$. The basic intuition is that for $\mu^\star \neq 0$, choosing b small enough guarantees a negative eigenvalue in $L(\mu^\star)$ independently of the choice of $\mu^\star \in S^T\Phi$, and for $\mu^\star = 0$, $L(\mu^\star)$ is a weighted Laplacian with positive weights which has $n-1$ positive eigenvalues whenever $\mathbb{G}$ is connected.

Let us now consider an equilibrium $(\mu^\star, 0)$ of the nonlinear system (65), (66). Recall that $L(\mu^\star)$ is congruent to $\mathrm{diag}\{0, L^\flat(\mu^\star)\}$; thus, Theorem 8, together with Sylvester's law of inertia, imply that $L^\flat(\mu^\star) > 0$ when $\mu^\star = 0$ and that $L^\flat(\mu^\star)$ has a negative eigenvalue for all nonzero $\mu^\star \in S^T\Phi$. Therefore, if $\mu^\star = 0$, which represents an in-phase steady-state solution, then it follows from Theorem 7 that this equilibrium is exponentially stable. Likewise, if $\mu^\star \neq 0$, which represents an out-of-phase steady-state solution, then this equilibrium is exponentially unstable. Because all out-of-phase equilibria are both isolated and exponentially unstable, we conclude (say from [39, Prop. 1], for example) that the set $\mathcal{S}_r \subset \mathbb{T}^n \times \Xi_r$ of initial states from which trajectories converge to out-of-phase steady-state solutions has zero measure in $\mathbb{T}^n \times \Xi_r$ (regarded here as a $(2n-1)$-dimensional manifold). It then follows from Tonelli's theorem that the set $\mathcal{S} = \bigcup_{r\in\mathbb{R}} \mathcal{S}_r$ has zero measure in $\mathbb{T}^n \times \mathbb{R}^n$. In other words, the system achieves asymptotic phase synchronization from almost every initial state.

V. Proof of Theorem 3

We define the diagonal matrix function

$$H(\gamma) = \mathrm{diag}\{\eta_1(\gamma), \ldots, \eta_m(\gamma)\} \in \mathbb{R}^{m\times m} \quad (78)$$

so that we can write the dynamics (24), (25) as

$$\dot{\varphi} = \Sigma(\gamma) \quad (79)$$
$$\dot{\gamma} = Ce(\varphi) - CBH(\gamma)B^T\Sigma(\gamma). \quad (80)$$

Because $\mathbf{1}_n^T e \equiv 0 = \mathbf{1}_n^T B$, the derivative of (43) along trajectories of (79) and (80) is

$$\dot{U} = -\Sigma^T(\gamma)BH(\gamma)B^T\Sigma(\gamma). \quad (81)$$

Now $H(\cdot)$ is positive definite; hence, $\dot{U} \leqslant 0$ and $\dot{U} = 0$ if and only if $B^T\Sigma(\gamma) = 0$. It follows from the Krasovskii-LaSalle invariance theorem that all trajectories of the system (79), (80) converge to the largest invariant set $\mathcal{M}$ contained within the set $\mathbb{T}^n \times \Gamma$, where $\Gamma \subset \mathbb{R}^n$ is from (47). We next show that again $\mathcal{M} = \Phi \times \Gamma$, just as in the proof of Theorem 2.

It follows from (80) that this systems also satisfies $q^T\dot{\gamma} \equiv 0$ and, thus, admits a foliation whose leaves are the invariant manifolds $\mathbb{T}^n \times \Xi_r$. Because $B^T\Sigma(\gamma)$ is the constant zero on the set Γ, its derivative is zero on $\mathcal{M}$

$$\begin{aligned} 0 &\equiv B^T\Sigma'(\gamma)\dot{\gamma} \equiv B^T\Sigma'(\gamma)QQ^T\dot{\gamma} \\ &\equiv B^TRS^T\Sigma'(\gamma)CS(S^TC^2S)^{-\frac{1}{2}}Q^T\dot{\gamma}. \end{aligned} \quad (82)$$

Because the columns of B^TR and S are independent and because the diagonal matrix $\Sigma'(\gamma)C$ is positive definite, it follows that $Q^T\dot{\gamma} \equiv 0$ and, thus, $\dot{\gamma} \equiv 0$ on $\mathcal{M}$. It then follows from (80) that $e(\varphi) \equiv 0$ on $\mathcal{M}$, and we conclude that $\mathcal{M} \subset \Phi \times \Gamma$. We observe that $\Phi \times \Gamma$ is itself invariant under the dynamics (79), (80), and it follows that $\mathcal{M} = \Phi \times \Gamma$.

We now fix $r \in \mathbb{R}$ and examine the dynamics on the invariant manifold $\mathbb{T}^n \times \Xi_r$. Using (63), we see that the derivatives of the projected state variables (64) along the trajectories of (79) and (80) are

$$\dot{w}_1 = S^T\Sigma(Qw_2 + \alpha_r) \quad (83)$$
$$\dot{w}_2 = Q^TCe(Rw_1) - Q^TCBH(Qw_2+\alpha_r) \times B^T\Sigma(Qw_2+\alpha_r). \quad (84)$$

As in the proof of Theorem 2, the equilibria of this system are precisely all points of the form $(\mu^\star, 0)$ for vectors $\mu^\star \in S^T\Phi$. The equilibrium with $\mu^\star = 0$ represents a fully synchronized trajectory with $\delta\varphi \equiv 0$, and all other equilibria represent out-of-phase, frequency-synchronized trajectories. Because $\mathcal{M} = \Phi \times \Gamma$, because $\Gamma \cap \Xi_r$ is a Singleton, and because the points of $S^T\Phi$ are isolated, we see that each trajectory of the system (83), (84) converges to an equilibrium.

We still have to perform a local linearization analysis at each equilibrium $(\mu^\star, 0)$ of the system (83), (84). We omit the details, but we can do this using Theorem 8 together with a dual version of Theorem 7 based on [40, Theor. 5, Corollary 2] (c.f. [38, Theor. 10]). The rest of the proof follows that of Theorem 2.

VI. Concluding Remarks

We have presented two distributed controllers for the phase and frequency synchronization of heterogeneous nonlinear oscillators, and we have shown that each guarantees almost-global convergence on arbitrary connected graphs. Our solutions can be readily implemented using analog oscillators and phase comparators, and our analysis holds under very general assumptions on the system. In particular, unlike most existing work, we neither require the set of admissible frequencies to be unbounded, nor assume any special network topology.

Appendix
Proof of Theorem 4

We let $\mathcal{T}$ denote the finite collection of all $m \times m$ diagonal matrices $\Delta = \mathrm{diag}\{\delta_1, \ldots, \delta_m\}$ such that for all $k \in \mathcal{E}$, either $\delta_k = f'(0)$ or $\delta_k = f'(\pi)$. For each such matrix $\Delta \in \mathcal{T}$, we define the closed set

$$\mathcal{P}_\Delta = \left\{a \in \mathbb{R}^m : \det\left(R^T B \mathrm{diag}(a) \Delta B^T R\right) = 0\right\} \quad (85)$$

where $\mathrm{diag}(a) = \mathrm{diag}\{a_1, \ldots, a_m\}$ denotes the diagonal matrix whose diagonal entries are the m elements of a. Now Δ is invertible by assumption **A5**), and furthermore, the columns of $B^T R$ are independent; it follows that $\mathcal{P}_\Delta \neq \mathbb{R}^m$ (take $\mathrm{diag}(a) = \Delta^{-1}$), which means $\mathcal{P}_\Delta$, is a closed algebraic set having zero measure. Thus

$$\mathcal{P} = \bigcup_{\Delta \in \mathcal{T}} \mathcal{P}_\Delta \quad (86)$$

is also a closed algebraic set having zero measure. Therefore, the set $\mathcal{O} = \mathbb{R}^m \setminus \mathcal{P}$ is a nonempty open semialgebraic set. Next, we define the mapping $\mathcal{H} : \mathbb{T}^{n-1} \times \mathcal{O} \to \mathbb{R}^{n-1}$ by

$$\mathcal{H}(\mu, a) = R^T B \mathrm{diag}(a) F(B^T R \mu). \quad (87)$$

The Jacobian matrix of $\mathcal{H}$ is

$$D\mathcal{H}(\mu, a) = \left[\frac{\partial \mathcal{H}}{\partial \mu}(\mu, a) \quad \frac{\partial \mathcal{H}}{\partial a}(\mu, a)\right] \quad (88)$$

where

$$\frac{\partial \mathcal{H}}{\partial \mu}(\mu, a) = R^T B \mathrm{diag}(a) F'(B^T R \mu) B^T R \quad (89)$$

$$\frac{\partial \mathcal{H}}{\partial a}(\mu, a) = R^T B \mathrm{diag}\left(F(B^T R \mu)\right). \quad (90)$$

If we define the matrix

$$\mathcal{J}(\mu, a) = \begin{bmatrix} I \\ \mathrm{diag}(a)\mathrm{diag}\left(F(B^T R \mu)\right)^+ \\ \cdot \left[F'(0) - F'(B^T R \mu)\right] B^T R \end{bmatrix} \quad (91)$$

where $(\cdot)^+$ denotes the Moore—Penrose pseudoinverse, then

$$D\mathcal{H}(\mu, a) \cdot \mathcal{J}(\mu, a) = R^T B \mathrm{diag}(a) \Delta(\mu) B^T R \quad (92)$$

where $\Delta(\mu)$ is the diagonal matrix

$$\Delta(\mu) = F'(B^T R \mu) + \mathrm{diag}\left(F(B^T R \mu)\right) \mathrm{diag}\left(F(B^T R \mu)\right)^+ \cdot \left[F'(0) - F'(B^T R \mu)\right]. \quad (93)$$

It follows from assumptions **A4**) and **A5**) that $f(\theta) = 0$ if and only if $\theta \in \{0, \pi\}$, so for any $\mu \in \mathbb{T}^{n-1}$, the matrix $\Delta(\mu)$ in (93) belongs to $\mathcal{T}$. It follows from the definition of $\mathcal{O}$ that the matrix in (92) is invertible, and we conclude that $D\mathcal{H}(\mu, a)$ has rank $n-1$ for all $(\mu, a) \in \mathbb{T}^{n-1} \times \mathcal{O}$. Thus, $\mathcal{H} \pitchfork \{0\}$,[3] and it follows from the parametric transversality theorem[4] [41, Theor. 6.35] that there exists a set $\mathcal{Y} \subset \mathcal{O}$ having zero measure such that if $a \in \mathcal{O} \setminus \mathcal{Y}$, then $\mathcal{H}_a \pitchfork \{0\}$, where $\mathcal{H}_a$ denotes the mapping $\mu \mapsto \mathcal{H}(\mu, a)$. Choose $\mathcal{Z} = \mathcal{P} \cup \mathcal{Y}$; we have thus shown that for all $a \in \mathbb{R}^m \setminus \mathcal{Z}$, if μ is such that $\mathcal{H}(\mu, a) = 0$, then the matrix in (89) is invertible. Note that we can also write $\mathcal{Z}$ as the projection of a closed subset of $\mathbb{T}^{n-1} \times \mathbb{R}^m$ onto $\mathbb{R}^m$ and, as such, it is closed because $\mathbb{T}^{n-1}$ is compact.

Suppose $a \in \mathbb{R}^m$ is the edge weight vector so that $A = \mathrm{diag}(a)$, suppose $a \in \mathbb{R}^m \setminus \mathcal{Z}$, and suppose $\mu \in S^T \Phi$. Then, $R\mu \in \Phi$ which means $\mathcal{H}(\mu, a) = 0$, and it follows that $L^\flat(\mu)$ in (51), which is the same as the matrix in (89), is invertible.

References

[1] S. Bregni, "A historical perspective on telecommunications network synchronization," *IEEE Commun. Mag.*, vol. 36, no. 6, pp. 158–166, Jun. 1998.

[2] W. Ye, J. Heidemann, and D. Estrin, "Medium access control with coordinated adaptive sleeping for wireless sensor networks," *IEEE/ACM Trans. Netw.*, vol. 12, no. 3, pp. 493–506, Jun. 2004.

[3] B. Sundararaman, U. Buy, and A. D. Kshemkalyani, "Clock synchronization for wireless sensor networks: A survey," *Ad Hoc Netw.*, vol. 3, no. 3, pp. 281–323, 2005.

[4] E. Mallada, X. Meng, M. Hack, L. Zhang, and A. Tang, "Skewless network clock synchronization," in *Proc. 21st IEEE Int. Conf. Netw. Protocols*, 2013, pp. 1–10.

[5] I. T. Union, "G. 812 timing requirements of slave clocks suitable for use as node clocks in synchronization networks," ITU, Geneva, Tech. Rep. E 26400, Jun. 1998.

[6] I. T. Union, "G. 811 Timing characteristics of primary reference clocks," ITU, Geneva, Tech. Rep. E 12242, Sep. 1997.

[7] H. Karl and A. Willig, *Protocols and Architectures for Wireless Sensor Networks*. Hoboken, NJ, USA: Wiley, 2007.

[8] A. T. Winfree, "Biological rhythms and the behavior of populations of coupled oscillators," *J. Theor. Biol.*, vol. 16, no. 1, pp. 15–42, 1967.

[9] Y. Kuramoto, "Cooperative dynamics of oscillator community a study based on lattice of rings," *Progr. Theor. Phys. Supplement*, vol. 79, pp. 223–240, 1984.

[10] R. E. Mirollo and S. H. Strogatz, "Synchronization of pulse-coupled biological oscillators," *SIAM J. Appl. Math.*, vol. 50, no. 6, pp. 1645–1662, 1990.

[11] Y. Kuramoto, *Chemical Oscillations, Waves, and Turbulence*. Berlin: Springer, 1984.

[12] A. Jadbabaie, J. Lin, and A. S. Morse, "Coordination of groups of mobile autonomous agents using nearest neighbor rules," *IEEE Trans. Autom. Control*, vol. 48, no. 6, pp. 988–1001, Jun. 2003.

[13] W. Ren, R. W. Beard, and E. M. Atkins, "Information consensus in multivehicle cooperative control," *IEEE Control Syst.*, vol. 27, no. 2, pp. 71–82, Apr. 2007.

[14] F. Tong and Y. Akaiwa, "Theoretical analysis of interbase-station synchronization systems," *IEEE Trans. Commun.*, vol. 46, no. 5, pp. 590–594, May 1998.

[15] O. Simeone and G. Scutari, "Pulse-coupled distributed PLLs in heterogeneous wireless networks," in *Proc. Conf. Rec. 41st Asilomar Conf. Signals, Syst. Comput.*, 2007, pp. 1770–1775.

[16] O. Simeone, U. Spagnolini, G. Scutari, and Y. Bar-Ness, "Physical-layer distributed synchronization in wireless networks and applications," *Phys. Commun.*, vol. 1, no. 1, pp. 67–83, 2008.

[3] If M and N are smooth manifolds, if $f : N \to M$ is smooth, and if S is an embedded submanifold of M, then f is *transverse to* S, written $f \pitchfork S$, when for every $p \in f^{-1}(S)$, we have $T_{f(p)}M = T_{f(p)}S + df_p(T_pN)$, where df_p denotes the differential of f at p.

[4] This transversality theorem is based on Sard's theorem, which holds only for sufficiently smooth functions. One can verify that in our case, this application of Sard's theorem is valid when the phase coupling function f is merely C^1.

[17] C. H. Rentel and T. Kunz, "A mutual network synchronization method for wireless *ad hoc* and sensor networks," *IEEE Trans. Mobile Comput.*, vol. 7, no. 5, pp. 633–646, May 2008.
[18] L. Schenato and F. Fiorentin, "Average TimeSynch: A consensus-based protocol for clock synchronization in wireless sensor networks," *Automatica*, vol. 47, no. 9, pp. 1878–1886, 2011.
[19] R. Carli, A. Chiuso, L. Schenato, and S. Zampieri, "A PI consensus controller for networked clocks synchronization," in *Proc. IFAC World Congr.*, 2008, pp. 10 289–10 294.
[20] R. Carli and S. Zampieri, "Networked clock synchronization based on second order linear consensus algorithms," in *Proc. 49th IEEE Conf. Dec., Control*, Dec. 2010, pp. 7259–7264.
[21] R. Carli, E. D'Elia, and S. Zampieri, "A PI controller based on asymmetric gossip communications for clocks synchronization in wireless sensors networks," in *Proc. Joint 50th IEEE Conf. Dec. Control Eur. Control Conf.*, Dec. 2011, pp. 7512–7517.
[22] R. Carli and S. Zampieri, "Network clock synchronization based on the second-order linear consensus algorithm," *IEEE Trans. Autom. Control*, vol. 59, no. 2, pp. 409–422, Feb. 2014.
[23] O. Simeone, U. Spagnolini, Y. Bar-Ness, and S. H. Strogatz, "Distributed synchronization in wireless networks," *IEEE Signal Process. Mag.*, vol. 25, no. 5, pp. 81–97, Sep. 2008.
[24] R. Carareto, F. M. Orsatti, and J. R. C. Piqueira, "Architectures, stability and optimization for clock distribution networks," *Commun. Nonlinear Sci. Numer. Simul.*, vol. 17, no. 12, pp. 4672–4682, Dec. 2012.
[25] J. Lunze, "Complete synchronization of Kuramoto oscillators," *J. Phys. A: Math. Theor.*, vol. 44, no. 42, 2011, Art. ID. 425102.
[26] Y.-W. Hong and A. Scaglione, "Time synchronization and reach-back communications with pulse-coupled oscillators for uwb wireless *ad hoc* networks," in *Proc. IEEE Conf. Ultra Wideband Syst. Technol.*, 2003, pp. 190–194.
[27] D. Lucarelli and I.-J. Wang, "Decentralized synchronization protocols with nearest neighbor communication," in *Proc. 2nd Int. Conf. Embedded Netw. Sens. Syst.*, 2004, pp. 62–68.
[28] X. Y. Wang, R. K. Dokania, and A. Apsel, "Pco-based synchronization for cognitive duty-cycled impulse radio sensor networks," *IEEE Sens. J.*, vol. 11, no. 3, pp. 555–564, Mar. 2011.
[29] E. Mallada and A. Tang, "Synchronization of weakly coupled oscillators: Coupling, delay and topology," *J. Phys. A: Math. Theor.*, vol. 46, no. 50, Dec. 2013, Art. ID. 505101.
[30] F. M. Gardner, *Phaselock Techniques*, 2nd ed. New York, NY, USA: Wiley, 1979.
[31] C. J. Byrne, "Properties and design of the phase-controlled oscillator with a sawtooth comparator," *Bell Syst. Tech. J.*, vol. 41, no. 2, pp. 559–602, 1962.
[32] V. Gutnik and A. Chandrakasan, "Active ghz clock network using distributed plls," in *Proc. IEEE Int. Solid-State Circuits Conf. Dig. Tech. Papers*, Feb. 2000, pp. 174–175.
[33] F. Dörfler and F. Bullo, "Synchronization in complex networks of phase oscillators: A survey," *Automatica*, May 2014.
[34] Y. Kuramoto, "Self-entrainment of a population of coupled non-linear oscillators," in *International Symposium on Mathematical Problems in Theoretical Physics*, vol. 39, H. Araki, Ed. New York, NY, USA: Springer-Verlag, 1975, ser. Lecture Notes in Physics, pp. 420–422.
[35] P. Monzón and F. Paganini, "Global considerations on the Kuramoto model of sinusoidally coupled oscillators," in *Proc. 44th IEEE Conf. Dec. Control Eur. Control Conf.*, 2005, pp. 3923–3928.
[36] E. Mallada and A. Tang, "Synchronization of phase-coupled oscillators with arbitrary topology," in *Proc. Amer. Control Conf.*, Jun. 2010, pp. 1777–1782.
[37] E. Mallada and A. Tang, "Distributed clock synchronization: Joint frequency and phase consensus," in *Proc. Joint 50th IEEE Conf. Dec. Control Eur. Control Conf.*, Dec. 2011, pp. 6742–6747.
[38] E. Mallada, R. A. Freeman, and A. Tang, "Distributed synchronization of heterogeneous oscillators on networks with arbitrary topology," *arXiv preprint arXiv:1405.6467*, 2014.
[39] R. A. Freeman, "A global attractor consisting of exponentially unstable equilibria," in *Proc. Amer. Control Conf.*, Jun. 2013, pp. 4862–4867.
[40] D. Carlson and H. Schneider, "Inertia theorems for matrices: The semidefinite case," *Bull. Amer. Math. Soc.*, vol. 68, no. 5, pp. 479–483, 1962.
[41] J. M. Lee, *Introduction to Smooth Manifolds*, vol. 218. New York, NY, USA: Springer-Verlag, 2012, ser. Graduate Texts in Mathematics.

Enrique Mallada (S'09–M'13) received the Ingeniero en Telecommunications degree from Universidad ORT, Montevideo, Uruguay, in 2005 and the Ph.D. degree in electrical and computer engineering with a minor in applied mathematics from Cornell University, Ithaca, NY, USA, in 2014.

Currently, he is a Postdoctoral Fellow in the Center for the Mathematics of Information (CMI) at the California Institute of Technology, Pasadena, CA, USA. His research interests include networks, control, nonlinear dynamics and optimization, with applications to power and information systems.

Dr. Mallada was a recipient of the Organization of American States (OAS) Academic Scholarship from 2008 to 2010, the Jacobs Fellowship from Cornell University in 2011, and the Cornell ECE Director's Thesis Research Award in 2014.

Randy A. Freeman received the Ph.D. degree in electrical engineering from the University of California at Santa Barbara, Santa Barbara, CA, USA, in 1995.

Since then, he has been a Faculty Member with Northwestern University, Evanston, IL, USA, where he is currently a Professor of Electrical Engineering and Computer Science. He has been Associate Editor of the IEEE TRANSACTIONS ON AUTOMATIC CONTROL. His research interests include nonlinear systems, distributed control, multiagent systems, robust control, optimal control, and oscillator synchronization.

Prof. Freeman received the National Science Foundation CAREER Award in 1997. He has been a member of the IEEE Control System Society Conference Editorial Board since 1997, and has served on program and operating committees for the American Control Conference and the IEEE Conference on Decision and Control.

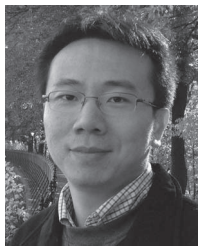

Ao Kevin Tang (S'01–M'07–SM'11) received the B.E. (Hons.) in electronics engineering from Tsinghua University, Beijing, China, in 1999, and the M.S. and Ph.D. degrees in electrical engineering with a minor in applied and computational mathematics from the California Institute of Technology, Pasadena, CA, USA, in 2002 and 2006, respectively.

Currently, he is an Associate Professor in the School of Electrical and Computer Engineering at Cornell University, Ithaca, NY, USA, where he conducts research on the control and optimization of engineering networks, including communication networks, power networks, and on-chip networks.

Dr. Tang's recent awards include the Cornell Engineering School Michael Tien'72 Excellence in Teaching Award in 2011, the Young Investigator Award from the Airforce Office of Scientific Research (AFOSR) in 2012, and the Presidential Early Career Award for Scientists and Engineers (PECASE) from the White House in 2012.